Journal of Fluids and Structures (2002) **16**(7), 891–907
doi:10.1006/jfls.460 available online at http://www.idealibrary.com on IDEAL®

AN EXPERIMENTAL STUDY ON THE FLUIDELASTIC FORCES ACTING ON A SQUARE TUBE BUNDLE IN TWO-PHASE CROSS-FLOW

F. Inada, K. Kawamura, A. Yasuo and K. Yoneda

Central Research Institute of Electric Power Industry (CRIEPI)
2-11-1, Iwado-Kita, Komae-shi, Tokyo 201-8511, Japan

(Received 17 May 2001; and in final form 22 March 2002)

A tube in a square tube bundle of $P/D = 1{\cdot}42$ was oscillated in the lift direction in air–water two-phase cross-flow, and fluidelastic forces acting on the oscillated tube were measured. First, the tube amplitude was fixed to 3 mm ($=0{\cdot}136D$), and added mass, damping, and stiffness coefficients were obtained as a function of two-phase mixture characteristics such as nondimensional gap velocity and void fraction. When reference mixture density and velocity were estimated, the drift–flux model, in which the relative velocity between the gas and liquid phases was estimated, generated better results than the homogeneous model. The added mass coefficient was obtained from quiescent two-phase flow as a function of void fraction. Using the added mass coefficient, the added stiffness coefficient converged to zero with decreasing nondimensional gap velocity. This overcame the contradiction in the added stiffness estimation without added mass, in which the added stiffness coefficient did not converge to zero with decreasing nondimensional gap velocity. Next, the effects of the vibration amplitude on the fluidelastic force coefficients were considered. When the tube amplitude was 3 mm ($=0{\cdot}136D$) or less, the equivalent added stiffness and damping coefficients were almost constant and nonlinearity was small. This showed the validity of the fluidelastic force coefficients obtained based on the data of amplitude of 3 mm. The linearity did not exist when the tube displacement amplitude was 4·5 mm ($=0{\cdot}205D$) or more; a remarkable nonlinearity appeared in the equivalent added damping coefficient. A method to estimate the limit-cycle amplitude of the fluidelastic vibration was proposed when only one tube in the tube bundle was able to vibrate in the lift direction. The amplitude could be obtained from the amplitude at which the equivalent added damping coefficient changed from negative to positive with increase in the tube amplitude.

1. INTRODUCTION

Fluidelastic vibration of a tube bundle in two-phase cross-flow has been observed in many shell-and-tube heat exchangers, and has been studied by several authors.

Axisa *et al*. (1984), Nakamura *et al*. (1986*a*, *b*, 1992, 1995), and Pettigrew *et al*. (1989*a*) researched the critical gap velocity. The stability boundary was estimated on the diagram of mass-damping parameter versus nondimensional gap velocity in the same manner as Connors' diagram (Connors 1970) for single-phase flow. Fluidelastic mass and/or damping were researched by Carlucci (1980), Carlucci & Brown (1983), Hara & Kohgo (1986), Pettigrew *et al*. (1989*b*), and Baj *et al*. (2002). These studies were reviewed in depth by Chen (1991), Hara (1993) and Pettigrew & Taylor (1994). However, the fluidelastic force characteristics were not clarified precisely in two-phase flow, in contrast to those in single-phase flow (Tanaka & Takahara 1981).

0889-9746/02/070891 + 17 $35.00/0

In addition, when the diagram of mass-damping parameter versus nondimensional gap velocity is used in two-phase flow, the characteristics of fluidelastic vibration are assumed to be expressed with two-phase mixture characteristics such as mixture density and mixture velocity, which are mainly obtained with the homogeneous two-phase flow model. It is necessary to consider whether the characteristics of fluidelastic vibration in two-phase cross-flow can be expressed with the two-phase mixture characteristics, because the time constant of the alternate phase change between gas and liquid can be comparable to the time constant of tube vibration. Furthermore, the homogeneous model can be improved to a more detailed model by considering the relative velocity between the gas and liquid phases to understand inherent characteristics in two-phase flow such as two-phase damping.

With this background, the authors (Inada *et al*. 1996, 1997) measured the fluidelastic forces acting on a square tube bundle of $P/D = 1{\cdot}42$ in air–water two-phase cross-flow when a tube in the tube bundle was oscillated at a displacement amplitude of 3 mm ($= 0{\cdot}136D$). However, it was not confirmed whether the linearity of fluidelastic forces remained up to the amplitude of 3 mm.

In this paper, the authors focus on the fluidelastic force acting on a tube that is oscillated in the lift direction. First, the characteristics of the fluidelastic force coefficients such as added mass, damping and stiffness coefficients are discussed when the amplitude of tube oscillation is 3 mm. It is shown that the drift–flux model (Zuber & Findlay 1965; Ishii 1977) generates better results than the homogeneous model when nondimensional coefficients are obtained. Second, the effect of the amplitude on the fluidelastic forces is examined experimentally. It is shown that the fluidelastic force is assumed to be linear when the amplitude is small. The factors controlling the amplitude are also considered.

2. EXPERIMENTAL APPARATUS

Figure 1 shows the test-section. Water is pumped through a surge tank, flow meter and valve, and flows into an air–water mixer. Air, which is compressed by a screw compressor, flows through a drier, a filter, a valve and a flow meter, and into the air–water mixer. In the air–water mixer, water flows perpendicularly to a tube bundle and air is discharged from the holes made in the wall of the tube bundle. The diameter of the holes is 0·5 mm. The air–water mixture made in the mixer flows through a flow rectifier consisting of a lattice with 30 mm gaps and 200 mm length, and into the tube bundle of the test-section. Here, the fluidelastic forces are measured.

The test-section has a rectangular tube bundle of 11 rows and 5 columns, with halftubes installed on either side of the channel wall. The diameter of each tube is 22 mm, the pitch is 31·3 mm, and the tube length is 198 mm. These tubes are made of aluminum alloy. The center tube in the sixth row can be oscillated with a motor–crank mechanism in the direction of the x- or y-axis. The angular frequency of the tube vibration is assumed to be Ω. The tube oscillated by the motor–crank mechanism is hollow to make the force of inertia small, but the other tubes are not. Fluidelastic forces can be measured with strain gauges installed near the base of the tubes, where the diameter is reduced to 10 mm. The fluidelastic force can be measured for four adjacent tubes of the oscillated tube, as well as for the oscillated tube itself, in the direction of the x- and y-axis. In this paper, only the fluidelastic force acting on the oscillated tube is obtained when the tube is oscillated in the x-direction, i.e., the lift direction. The natural frequencies of the tubes are larger than 150 Hz, and the fluidelastic force can be measured when the oscillation frequency is < 25 Hz.

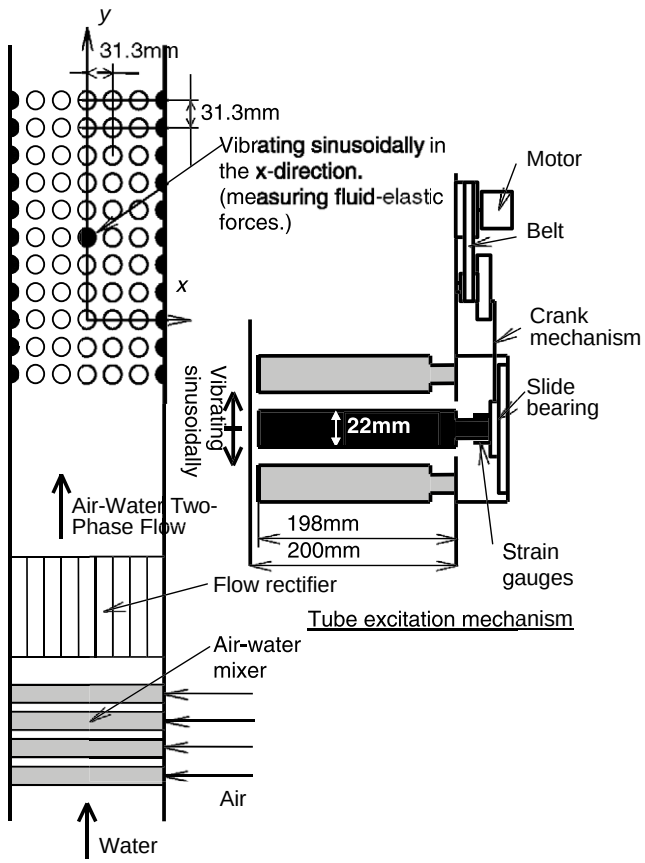

Figure 1. Test-section of the experimental apparatus.

3. RESULTS OF FLUIDELASTIC FORCE COEFFICIENTS

3.1. Experimental Conditions

The frequency of the tube vibration is changed from 5 to 25 Hz, water velocity at the gap from 0 to 6 m/s and air velocity at the gap from 0 to 7·5 m/s. In this case, the void fraction is lower than 0·8. The amplitude of the tube is fixed at 3 mm ($=0{\cdot}136D$).

3.2. Data Reduction

Each fluidelastic coefficient, such as added mass, damping and stiffness coefficient, is obtained when tube displacement amplitude, fluidelastic force amplitude, and phase difference between the tube displacement and fluid force are measured. The tube displacement is obtained using an acceleration pick-up of a strain-gauge type. The tube displacement and fluid force amplitudes, x_{0-p} and $F_{xox,0-p}$, are obtained when the root-mean-square value is calculated from integration of the power spectral density and the wave shape of both the tube displacement and fluid force are assumed to be sinusoidal. The data are collected for 64 s. The power spectral densities of tube displacement and fluidelastic force, an example of which is shown in Figure 2, had a sharp peak at the

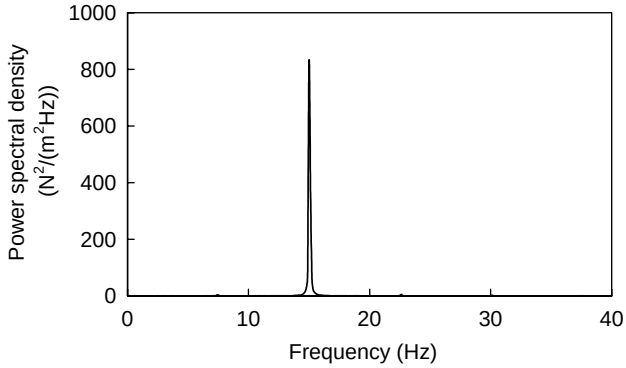

Figure 2. Example of the power spectral density of the fluidelastic force, for $\alpha = 0{\cdot}4$, $x_{0-p} = 3\,\text{mm}$, $j_L = 1{\cdot}67\,\text{m/s}$, $V_R = 1{\cdot}64$.

excitation frequency. Regarding the fluidelastic force, the power spectral density includes random flow excitation force components, and integration is conducted in the region of excitation frequency $\pm 0{\cdot}5\,\text{Hz}$. Of course, random flow excitation force is included in this frequency region. The ratio of random flow excitation force amplitude to fluidelastic force amplitude was $<5\%$ when the excitation frequency was 20 Hz, gas velocity was about 1 m/s, and liquid velocity was about 2 m/s. The mass of the test cylinder can also generate the force proportional to the tube acceleration. So, the mass of the test cylinder was obtained when the center tube was oscillated at several frequencies in air. The result was 0·22 kg/m. The inertia force due to the test cylinder was subtracted from the total force. The added mass in single-phase water is around 0·8 kg/m, which is four times larger than the mass of the test cylinder. Even if the decrease of the added mass in two-phase flow is taken into account, the error generated by the uncertainty of the mass of the test cylinder can be small.

The phase delay of the fluidelastic force from tube displacement, ϕ, is obtained from the argument of cross-spectral density at the excitation frequency.

Added mass, damping, and stiffness coefficients are obtained as follows:

$$K_{axox} - M_{axox}\Omega^2 = (F_{xox,0-p}/x_{0-p})\cos\phi, \qquad \Omega C_{axox} = -(F_{xox,0-p}/x_{0-p})\sin\phi. \quad (1)$$

3.3. Experimental Results

3.3.1. Definition of two-phase flow parameters

In the drift–flux model, the gas velocity u_G is expressed as:

$$u_G = C_0 j_T + V_{Gj}, \quad (2)$$

where volumetric flux densities of gas, liquid and mixture are defined by

$$j_G = \alpha u_G, \qquad j_L = (1-\alpha)u_L, \qquad j_T = j_G + j_L \quad (3)$$

with C_0 being the distribution parameter and V_{Gj} the drift velocity. The parameters C_0 and V_{Gj} depend on the flow pattern, and generally can be calculated from the experimental data of gas velocity as a function of volumetric flux density of the mixture. In the case of flow in a circular pipe, when the void fraction is between 0·5 and 0·8 in a 25·4 mm diameter tube, the flow regime is called *churn turbulent flow*. This regime is between slug flow and

annular flow. C_0 and V_{Gj} are obtained experimentally as follows (Ishii 1977):

$$C_0 = 1{\cdot}2 - 0{\cdot}2\sqrt{\frac{\rho_G}{\rho_L}}, \qquad V_{Gj} = \sqrt{2}\left[\frac{\sigma g(\rho_L - \rho_G)}{\rho_L^2}\right]^{0{\cdot}25}. \tag{4}$$

In the case of the tube bundle, there are no data available. The flow through the tube bundle may be close to churn turbulent because the flow is stirred up by the tube bundle. Hence, equation (4) is used for a first-step estimation. However, the flow inside a tube bundle can be significantly different from the flow inside a circular pipe, and when vibration of tube bundles is discussed using the drift–flux model, the flow regime in the tube bundle should be considered in the future.

Using j_G and j_L, mass flux is expressed as

$$G = \rho_G j_G + \rho_L j_L. \tag{5}$$

In the homogeneous model, the homogeneous void fraction, mixture density and mixture gap velocity are defined by

$$\beta = j_G/j_T, \qquad \rho_H = \rho_G\beta + \rho_L(1-\beta), \qquad U_{gH} = G/\rho_H. \tag{6}$$

In the drift–flux model, the mixture density and mixture gap velocity are defined by

$$\rho = \rho_G\alpha + \rho_L(1-\alpha), \qquad U_g = G/\rho. \tag{7}$$

3.3.2. Definition of nondimensional parameters

The nondimensional gap velocity in the drift–flux model and homogeneous model is defined by

$$V_R = \frac{U_g}{\Omega D}, \qquad V_{RH} = \frac{U_{gH}}{\Omega D}, \tag{8}$$

and the nondimensional added mass, damping and stiffness coefficients in the drift–flux model and homogeneous model are defined by

$$\hat{M}_{axox} = \frac{M_{axox}}{\rho D^2/2}, \qquad \hat{C}_{axox} = \frac{C_{axox}}{\rho D^2\Omega/2}, \qquad \hat{K}_{axox} = \frac{K_{axox}}{\rho D^2\Omega^2/2},$$
$$\hat{M}_{aHxox} = \frac{M_{axox}}{\rho_H D^2/2}, \qquad \hat{C}_{aHxox} = \frac{C_{axox}}{\rho_H D^2\Omega/2}, \qquad \hat{K}_{aHxox} = \frac{K_{axox}}{\rho_H D^2\Omega^2/2}. \tag{9}$$

3.3.3. Homogeneous model and drift–flux model

We first discuss whether or not better results can be derived from the drift–flux model than the homogeneous model. The added stiffness coefficient is shown in nondimensional form in Figures 3 and 4. Figure 3 shows the results estimated with the drift–flux model, and Figure 4 shows the results estimated with the homogeneous model. The comparison between the two models was done with almost the same data points. If the flow conditions are the same, V_{RH} becomes larger than V_R, so the range of the horizontal axis of Figure 4 is larger than that of Figure 3. In Figure 3, the solid line shows a trend line obtained by using regression analysis. In previous reports (Inada *et al.* 1996, 1997), the added stiffness coefficient was shown for a wide range of nondimensional gap velocity up to 100. We do not need to estimate the coefficient for such a wide range in engineering, as the accuracy of fit is not good when fitting data in a curve over such a wide range. In this report, the range of nondimensional gap velocity is limited to 3 or less. When the flow is estimated with the homogeneous model, the scatter of data is large. However, when the flow is estimated with

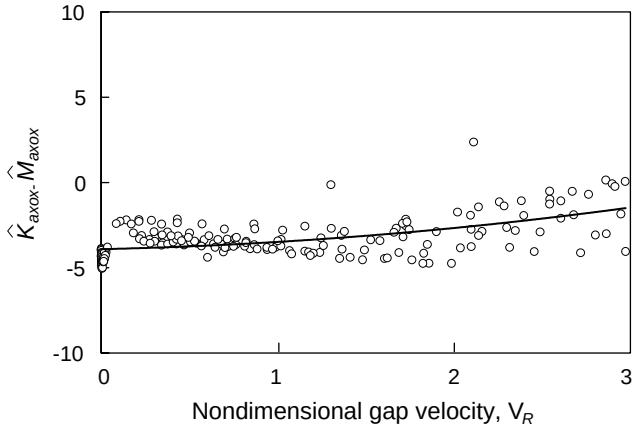

Figure 3. Nondimensional added stiffness coefficient estimated with the drift–flux model.

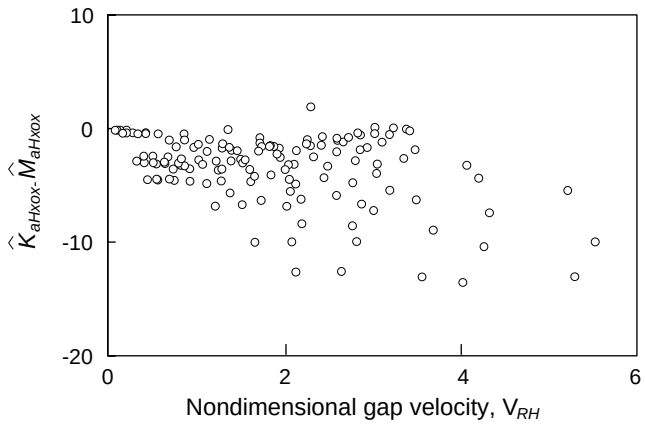

Figure 4. Nondimensional added stiffness coefficient estimated with the homogeneous model.

the drift–flux model, the data collapse very well, which shows that the drift–flux model generates better results than the homogeneous model.

3.3.4. Added stiffness and added mass coefficient

In Figure 3, even if the nondimensional gap velocity approaches zero, the added stiffness coefficient does not converge to zero, which is incorrect from the standpoint of physics. Next, the gap from zero in the low nondimensional gap velocity region will be reduced by introducing the added mass coefficient. When the added mass coefficient is obtained experimentally, the phase difference of fluid force due to added mass and that due to added stiffness is 180°, as shown by equation (1). We should consider how to separate them.

In this report, when liquid velocity is zero and only gas flows, i.e., for a quiescent two-phase flow, the added stiffness is assumed to be zero and the entire component proportional to the acceleration of the tube is assumed to be the added mass, because the density of the gas is much lower than that of the liquid. This means that the contribution of gas flow to the fluid force is very small. The absence of liquid in the gas phase is

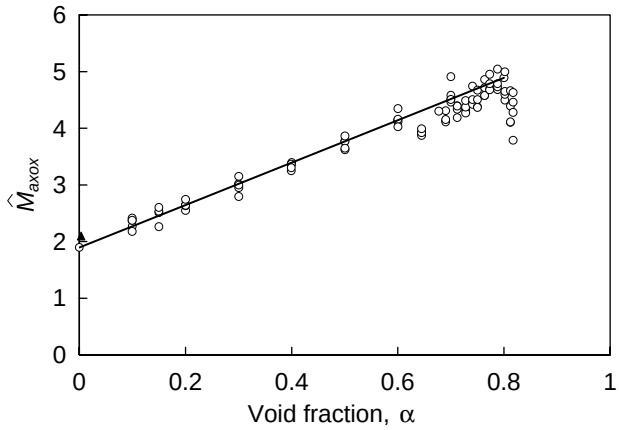

Figure 5. Nondimensional added mass coefficient: ▲, Pettigrew & Taylor (1994).

important in the case of gas–liquid two-phase flow, which induces only an added mass component.

The nondimensional added mass coefficient is shown in Figure 5. The data for various frequency conditions are plotted. The nondimensional added mass coefficient is independent of tube vibration frequency under this experimental condition. The nondimensional added mass coefficient increases with increasing void fraction when the void fraction is lower than 0·75; conversely, it decreases with increasing void fraction when the void fraction is higher than 0·75.

Incidentally, the added mass coefficient is nondimensionalized by $\frac{1}{2}\rho D^2$, where ρ is the mixture density. If we consider completely mixed two-phase flow, and it can be treated as if it were single-phase flow, then it is suggested that the nondimensional added mass becomes constant, and is independent of void fraction. However, Figure 5 shows that the nondimensional added mass coefficient depends on the void fraction, which suggests that the relative motion between the liquid and gas phases may affect the fluid dynamic force. Further study on this matter is required.

When the void fraction is zero, the result is consistent with that of previous research (Pettigrew & Taylor 1994) on single-phase flow.

Figure 6 shows the nondimensional added stiffness coefficient when the component of added mass is excluded. In Figure 6, the solid line shows a trend line obtained by using regression analysis. The added stiffness coefficient converges to zero when the nondimensional gap velocity approaches zero. The nondimensional added stiffness coefficient is positive, and increases with increasing nondimensional gap velocity.

3.3.5. Added damping coefficient and two-phase damping

Figure 7 shows the nondimensional added damping coefficient estimated with the drift–flux model where the solid line shows a trend line obtained by using regression analysis. The nondimensional added damping coefficient depends on void fraction α. In the case of $\alpha = 0$, the coefficient is negative, and the absolute value decreases monotonously from 0 with increasing nondimensional gap velocity, V_R. On the other hand, in the case of $\alpha > 0{\cdot}4$, the coefficient is positive and increases slightly with increasing V_R when V_R is small. When V_R becomes large, the nondimensional added damping coefficient decreases with

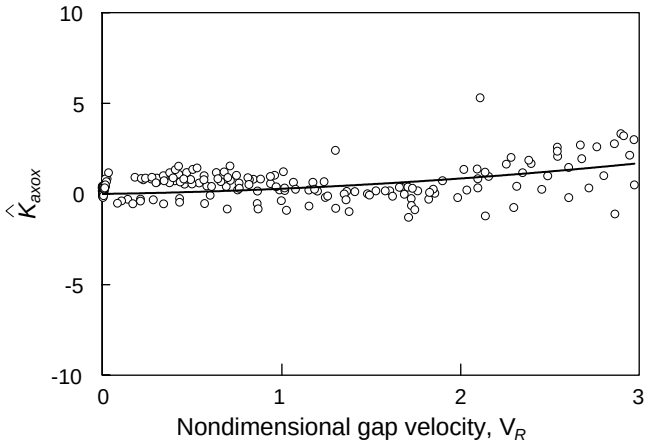

Figure 6. Nondimensional added stiffness coefficient excluding the added mass component.

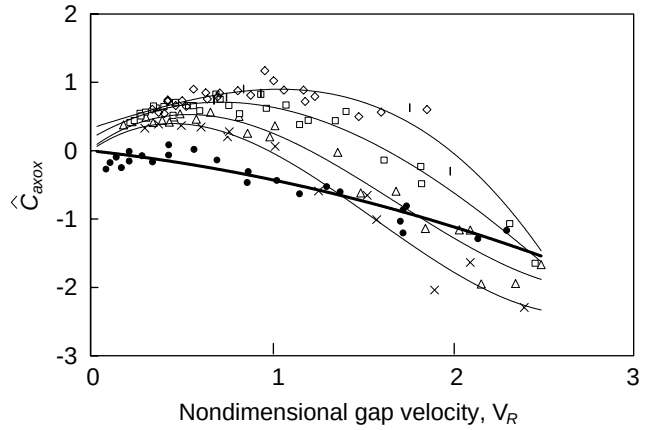

Figure 7. Nondimensional added damping coefficient estimated with the drift–flux model: •, $\alpha = 0$; ×, $0{\cdot}4 < \alpha < 0{\cdot}5$; △, $0{\cdot}5 < \alpha < 0{\cdot}6$; □, $0{\cdot}6 < \alpha < 0{\cdot}7$; ◊, $0{\cdot}7 < \alpha < 0{\cdot}8$.

increasing V_R, and becomes negative; the nondimensional gap velocity at which this occurs increases with increasing void fraction. The data collapse very well in each void fraction region. The results show the same trend as those of Baj *et al.* (2002), at least qualitatively.

Figure 8 shows the results estimated with the homogeneous model, where the solid line shows a trend line obtained by using regression analysis. The scatter of data is relatively large.

In Figure 7, the added damping coefficient becomes positive in the low nondimensional gap velocity region when $\alpha > 0{\cdot}4$, which means the existence of damping induced by two-phase flow.

Two-phase damping was first defined by Pettigrew & Taylor (1994), using the homogeneous model. In his theory, the total fluid damping ratio, ζ_{TF} in two-phase mixtures was divided into two-phase damping, ζ_{TP}, a viscous damping, ζ_v, and a

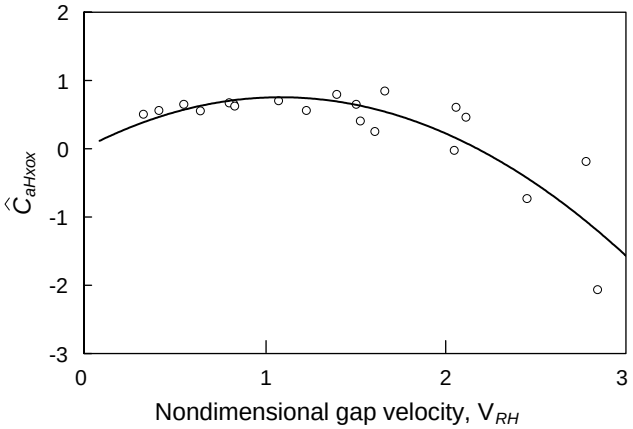

Figure 8. Nondimensional added damping coefficient estimated with the homogeneous model: $0{\cdot}7 < \beta < 0{\cdot}8$.

flow-dependent damping, ζ_{FD}, as follows:

$$\zeta_{TF} = \zeta_{TP} + \zeta_V + \zeta_{FD}. \tag{10}$$

In Pettigrew's (1994) work, two-phase damping was defined as the damping when the flow velocity is half the critical velocity of fluidelastic vibration. Figure 7 shows the existence of two-phase damping from an engineering perspective; however, a more reasonable explanation of added damping in two-phase flow should be considered.

4. DEPENDENCY OF FLUIDELASTIC FORCES ON VIBRATION AMPLITUDE

4.1. Experimental Conditions

The frequency of the tube vibration is fixed to 15 Hz. The water gap velocity is varied from 0 to 3 m/s and the air gap velocity from 0 to 3 m/s. In this case, the void fraction ranges from 0 to 70%. The amplitude of the tube is changed from 1·5 mm ($=0{\cdot}068D$) to 7 mm ($=0{\cdot}318D$).

4.2. Experimental Results of Fluidelastic Forces

The fluidelastic forces are measured in the same manner as in Section 3.

Figure 9 shows an example of the relation between excitation amplitude of the tube, x_{0-p}, and the amplitude of the excitation frequency component of the fluidelastic force, $F_{xox,0-p}$. Volumetric flux of liquid, j_L, which is the flow velocity when assuming that only liquid flows in the entire cross-section, is 1·67 m/s. The void fraction α is changed as a parameter. $F_{xox,0-p}$ is nearly proportional to the amplitude at least when the amplitude is 4·5 mm ($=0{\cdot}205D$) or less. Even if the amplitude is increased up to about 7 mm ($=0{\cdot}318D$), the degradation of the linear relation is small. The relation between x_{0-p} and $F_{xox,0-p}$ shows almost the same tendency when $j_L < 3{\cdot}2$ m/s.

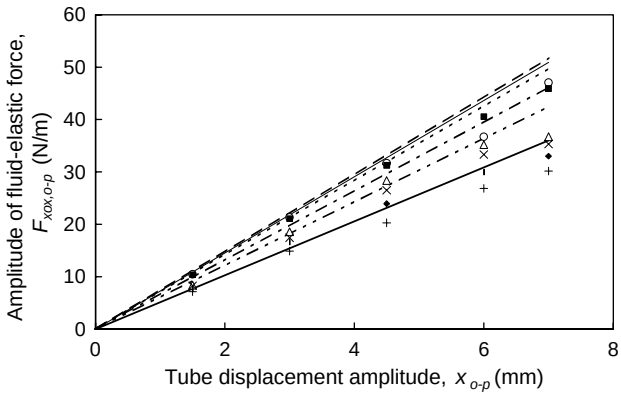

Figure 9. Example of the relation between excitation amplitude of the tube and the amplitude of fluidelastic force ($j_L = 1{\cdot}67$ m/s): ○, ——, $\alpha = 0{\cdot}2$; ■, – – -, $\alpha = 0{\cdot}3$; △, - - - -, $\alpha = 0{\cdot}4$; ×, – · – · –, $\alpha = 0{\cdot}5$; ◆, – ·· – ··, $\alpha = 0{\cdot}6$; +, $\alpha = 0{\cdot}7$.

The phase difference between the tube vibration and the fluidelastic force is shown in Figure 10 as a function of the amplitude of the tube. In Figure 10(a–c), j_L is 0, 0·4, and 0·81 m/s, respectively. The phase difference is negative at almost all amplitudes and is independent of the amplitude for $x_{0\text{–}p} < 6$ mm ($= 0{\cdot}273D$). When the phase difference is positive, the absolute value is small. In Figure 10(d), $j_L = 1{\cdot}19$ m/s. The phase difference is almost constant when the amplitude is $< 4{\cdot}5$ mm ($= 0{\cdot}205D$). When the amplitude is larger than 4·5 mm, the trend may be are divided into two groups: one in which the void fraction is $< 0{\cdot}3$ where the phase difference increases from negative to positive values, and the other in which the void fraction is more than 0·4 where the phase difference becomes negative and the absolute value increases.

In Figure 10(e), j_L is raised to 1·67 m/s. The phase difference becomes positive and does not depend on the amplitude so much when the amplitude is smaller than 3 mm ($= 0{\cdot}136D$). The phase difference becomes positive and increases with increase in the amplitude above 4·5 mm ($= 0{\cdot}205D$) when the void fraction is $< 0{\cdot}3$. When void fraction is larger than 0·4 and the amplitude is above 4·5 mm, the phase difference changes from positive to negative. It is found that the dependency of the phase difference on the amplitude becomes large under any void fraction conditions.

Figure 10(f) shows the case where j_L is raised to 3·2 m/s. The phase difference is positive and does not depend on the amplitude when the amplitude is smaller than 3 mm ($= 0{\cdot}136D$). When the amplitude is larger than 4·5 mm ($= 0{\cdot}205D$), the phase difference increases when the void fraction is $< 0{\cdot}3$, and decreases when the void fraction is larger than 0·4. The rate of decrease becomes larger with increasing void fraction.

Figure 10 shows that fluidelastic force is linear in engineering for the amplitude of 3 mm ($= 0{\cdot}136D$) or less in the range of the experimental flow rate conditions. This shows the validity of the fluidelastic coefficients in Section 3, in which the coefficients were obtained based on the data of amplitude of 3 mm.The principle of superposition is applicable for the amplitude of 3 mm or less. Therefore, the coefficients can be used to estimate stability around the equilibrium position for infinitesimally small perturbations. Linearity does not exist when the tube displacement amplitude is 4·5 mm ($= 0{\cdot}205D$) or more; a remarkable nonlinearity appears in the phase difference.

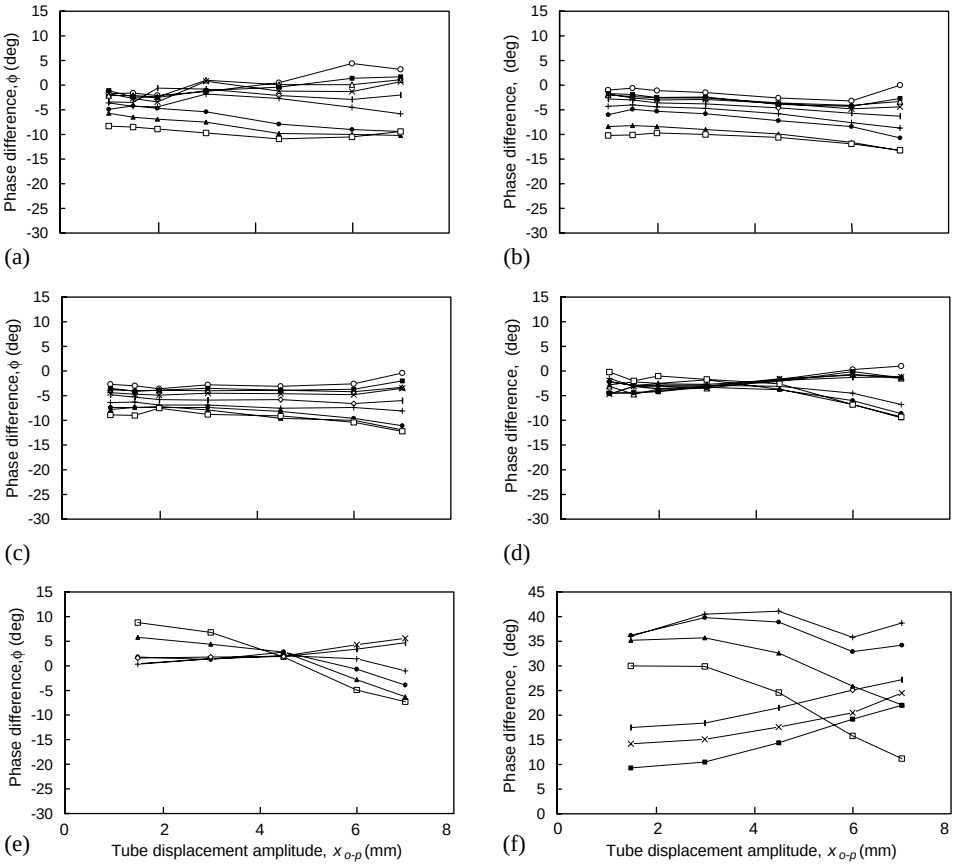

Figure 10. Phase difference between the tube vibration and the fluidelastic force: ○, $\alpha = 0$; ■, $\alpha = 0{\cdot}1$; △, $\alpha = 0{\cdot}15$; ×, $\alpha = 0{\cdot}2$; ◊, $\alpha = 0{\cdot}3$; +, $\alpha = 0{\cdot}4$; ●, $\alpha = 0{\cdot}5$; ▲, $\alpha = 0{\cdot}6$; □, $\alpha = 0{\cdot}7$. (a) $j_L = 0$ m/s; (b) $j_L = 0{\cdot}4$ m/s; (c) $j_L = 0{\cdot}81$ m/s; (d) $j_L = 1{\cdot}19$ m/s; (e) $j_L = 1{\cdot}67$ m/s; (f) $j_L = 3{\cdot}2$ m/s.

4.3. Equivalent Fluidelastic Force Coefficients

Though the amplitude of the fluidelastic force, $F_{xox,0-p}$, and the phase difference of the fluidelastic force to the tube vibration, ϕ, are shown in Figures 9 and 10, the physical meaning is not yet clear. So, let us obtain equivalent added stiffness coefficient, $K_{a\text{eq}}$, and equivalent added damping coefficient, $C_{a\text{eq}}$, from fluidelastic force using equation (1) as shown in Figures 11 and 12, where $K_{a\text{eq}}$ and $C_{a\text{eq}}$ are defined and nondimensionalized as follows:

$$K_{a\text{eq}} = (F_{xox,0-p}/x_{0-p})\cos\phi, \qquad \Omega C_{a\text{eq}} = -(F_{xox,0-p}/x_{0-p})\sin\phi, \tag{11}$$

$$\hat{C}_{a\text{eq}} = \frac{C_{a\text{eq}}}{\rho D^2 \Omega/2}, \qquad \hat{K}_{a\text{eq}} = \frac{K_{a\text{eq}}}{\rho D^2 \Omega^2/2}. \tag{12}$$

The variable ρ is the mixture density, and is obtained based on the drift-flux model. In equations (11) and (12), $K_{a\text{eq}}$ includes the added mass component.

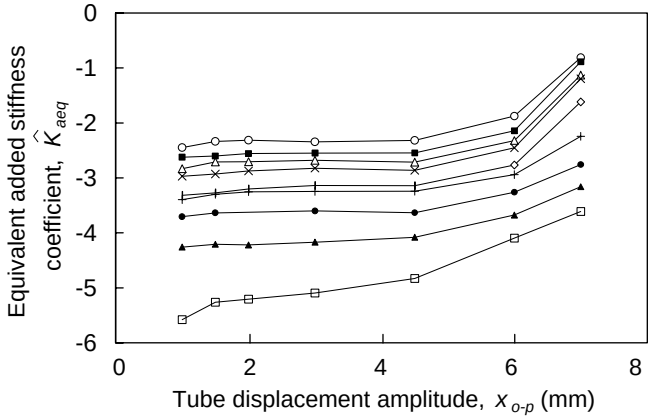

Figure 11. Example of the nondimensional equivalent added stiffness coefficient as a function of tube oscillation amplitude ($j_L = 1{\cdot}19$ m/s): ○, $\alpha = 0$; ■, $\alpha = 0{\cdot}1$; △, $\alpha = 0{\cdot}15$; ×, $\alpha = 0{\cdot}2$; ◊, $\alpha = 0{\cdot}3$; +, $\alpha = 0{\cdot}4$; ●, $\alpha = 0{\cdot}5$; ▲, $\alpha = 0{\cdot}6$; □, $\alpha = 0{\cdot}7$.

If both equivalent coefficients depend on the tube amplitude, added damping and stiffness coefficients are nonlinear. If both equivalent coefficients are independent of the tube amplitude at small amplitudes, added damping and stiffness coefficients are assumed to be linear. Now, let us consider the case in which only one tube in the tube bundle can vibrate and only in the lift direction. If we consider the case of small amplitude where fluidelastic force is linear, the added stiffness coefficient cannot be related to the mechanism of fluidelastic vibration, whereas the added damping coefficient can be related to the generation of fluidelastic vibration. The natural frequency increases for the positive added stiffness coefficient, and decreases for the negative added stiffness coefficient. Fluidelastic vibration can be generated, and the amplitude increases exponentially when the total damping coefficient of the structure and fluidelastic force is negative.

Figure 11 shows a nondimensional equivalent added stiffness coefficient, $\hat{K}_{a\mathrm{eq}}$, for the case of $j_L = 1{\cdot}19$ m/s as an example. It does not depend on the amplitude and is constant up to $x_{0\text{–}p} = 4{\cdot}5$ mm ($= 0{\cdot}205D$), in which $\hat{K}_{a\mathrm{eq}}$ is linear.

The nondimensional equivalent added damping coefficient, $\hat{C}_{a\mathrm{eq}}$, is shown in Figure 12. In Figure 12(a), $j_L = 0$. The value of $\hat{C}_{a\mathrm{eq}}$ can be negative in the small void fraction region. In this case, gas velocity is not so large, and negative added damping cannot be generated. The absolute value of negative damping is small, and may be due to experimental error. The value of $\hat{C}_{a\mathrm{eq}}$ is assumed to be near zero in this region. When the void fraction is 0·2 or more, $\hat{C}_{a\mathrm{eq}}$ is positive and almost linear. In Figure 12(b) and (c), j_L is 0·4 and 0·81 m/s, respectively. The value of $\hat{C}_{a\mathrm{eq}}$ is positive and independent of the amplitude, and fluidelastic vibration cannot occur.

In Figure 12(d), $j_L = 1{\cdot}19$ m/s. The value of $\hat{C}_{a\mathrm{eq}}$ is positive and almost constant when the void fraction is $< 4{\cdot}5$ mm ($= 0{\cdot}205D$). When the amplitude is larger than 4·5 mm, the trend is of two types: one in which the void fraction is $< 0{\cdot}3$ where $\hat{C}_{a\mathrm{eq}}$ decreases from a positive value to a very small value; the other in which the void fraction is more than 0·4, where $\hat{C}_{a\mathrm{eq}}$ is positive and the absolute value increases.

In Figure 12(e), j_L is raised to 1·67 m/s. The value of $\hat{C}_{a\mathrm{eq}}$ becomes negative and does not depend on the amplitude so much when the amplitude is smaller than 3 mm ($= 0{\cdot}136D$).

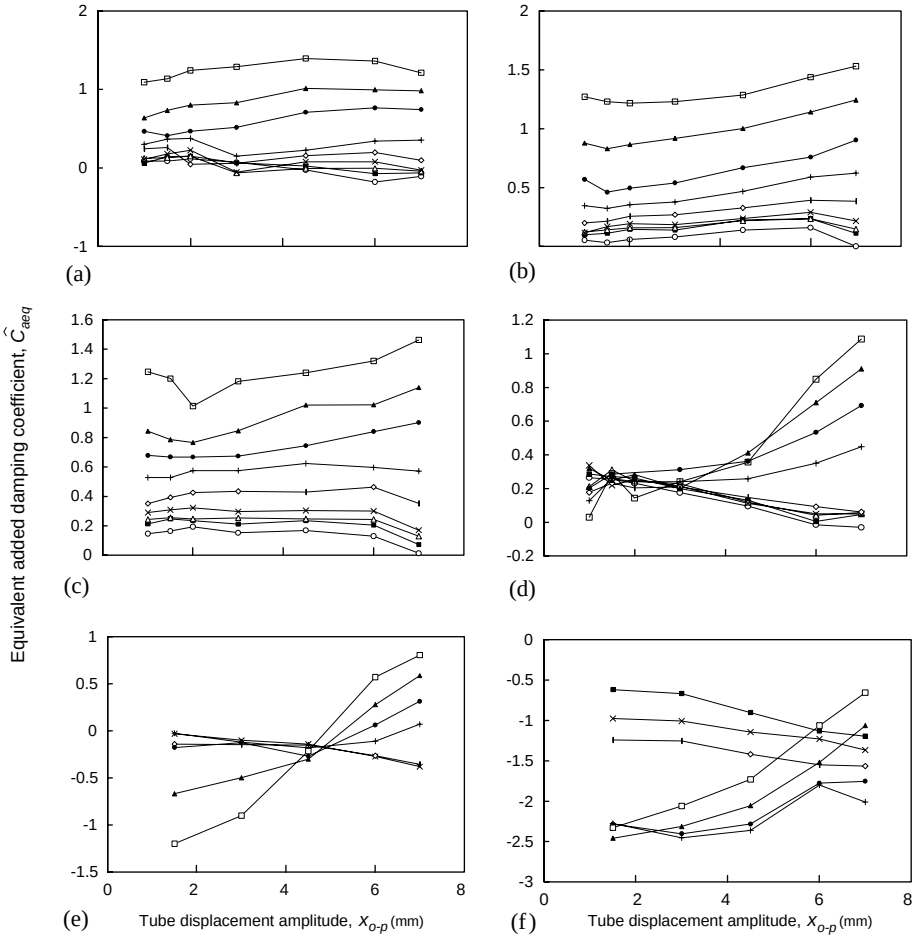

Figure 12. Nondimensional equivalent added damping coefficient as a function of the tube oscillation amplitude: ○, $\alpha = 0$; ■, $\alpha = 0{\cdot}1$; △, $\alpha = 0{\cdot}15$; ×, $\alpha = 0{\cdot}2$; ◊ $\alpha = 0{\cdot}3$; +, $\alpha = 0{\cdot}4$; ●, $\alpha = 0{\cdot}5$; ▲, $\alpha = 0{\cdot}6$; □, $\alpha = 0{\cdot}7$. (a) $j_L = 0$ m/s; (b) $j_L = 0{\cdot}4$ m/s; (c) $j_L = 0{\cdot}81$ m/s; (d) $j_L = 1{\cdot}19$ m/s; (e) $j_L = 1{\cdot}67$ m/s; (f) $j_L = 3{\cdot}2$ m/s.

The value of $\hat{C}_{a\text{eq}}$ becomes negative and the absolute value increases with increasing the amplitude above 4·5 mm ($=0{\cdot}205D$) when the void fraction is 0·3 or less. When the void fraction is larger than 0·4 and the amplitude is above 4·5 mm, the value of $\hat{C}_{a\text{eq}}$ changes from negative to positive. It is found that the dependency of $\hat{C}_{a\text{eq}}$ on the amplitude becomes large under any void fraction conditions.

Figure 12(f) shows the case where j_L is raised to 3·2 m/s. The value of $\hat{C}_{a\text{eq}}$ is negative and does not depend on the amplitude when the amplitude is smaller than 3 mm ($=0{\cdot}136D$). When the amplitude is larger than 4·5 mm ($=0{\cdot}205D$), $\hat{C}_{a\text{eq}}$ becomes negative and its absolute value (i) increases when the void fraction is $<0{\cdot}3$, and (ii) it decreases when the void fraction is larger than 0·4. The rate of decrease becomes larger with increasing void fraction.

Figure 12 also shows that the fluidelastic force is linear for engineering purposes, for an amplitude of 3 mm ($=0{\cdot}136D$) or less in the range of the experimental flow rate conditions. The linearity does not exist when the tube displacement amplitude $x_{0\text{–}p}$ is

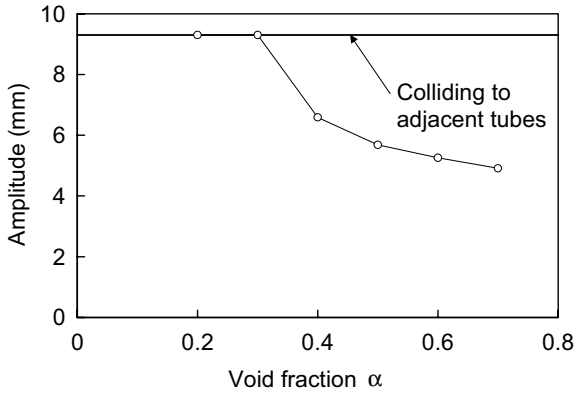

Figure 13. Example of the limit-cycle amplitude of fluidelastic vibration ($j_L = 1{\cdot}67$ m/s).

4·5 mm ($=0{\cdot}205D$) or more; a remarkable nonlinearity appears in the equivalent added damping coefficient.

4.4. Preliminary Amplitude Evaluation

The fluidelastic forces are nonlinear at large amplitudes, and the principle of superposition is not applicable. If it is considered that a single flexible tube can oscillate in a single direction in a rigid tube bundle, then the amplitude of the tube can be obtained from the fluidelastic force, because the force was obtained for a single oscillated tube in a rigid tube bundle. However, if all tubes are considered flexible, then the amplitude of the tube cannot be obtained.

Now, let us consider the case in which a tube in a tube bundle is able to vibrate only in the lift direction again. When the damping coefficient is negative, at infinitesimally small amplitude, fluidelastic vibration occurs. When the nondimensional equivalent damping coefficient, $\hat{C}_{a\mathrm{eq}}$, obtained from equation (11) changes from negative to positive with increasing the amplitude, the limit-cycle amplitude of the fluidelastic vibration is the point at which $\hat{C}_{a\mathrm{eq}}$ becomes zero. This principle is used in this section.

Figure 13 shows an example of the limit-cycle amplitude of fluidelastic vibration as a function of the void fraction when $j_L = 1{\cdot}67$ m/s. Since $\hat{C}_{a\mathrm{eq}}$ is always negative in the case of $\alpha < 0{\cdot}3$, the amplitude is assumed to grow until the tube collides with adjacent tubes. When the void fraction is 0·4 or more, the amplitude becomes small at about 4–5 mm ($=0{\cdot}18D$–$0{\cdot}23D$).

When j_L is 3·2 m/s, $\hat{C}_{a\mathrm{eq}}$ is always negative for an amplitude of 7 mm ($=0{\cdot}318D$) or less and the void fraction of 0·7 or less as shown in Figure 12(f). When the flow velocity is large, the vibration grows until the tube collides the adjacent tubes.

The evaluation method presented in this paper is applicable when the correlation length of the void fraction fluctuation in the axial direction is much shorter than 200 mm, which is the measurement length of fluidelastic force, and also much smaller than the length of the evaluated pipeline. However, data concerning the correlation length of void fraction fluctuations were not found in previous studies, and need to be gathered experimentally in the future. Experimental verifications of the amplitude evaluation are also necessary.

5. CONCLUSIONS

The fluidelastic forces acting on a square tube bundle in air–water two-phase cross-flow were measured when a tube in the tube bundle was oscillated in the lift direction. The results may be summarized as follows:

(i) Added mass, damping and stiffness coefficients were obtained as a function of two-phase mixture characteristics such as nondimensional gap velocity and void fraction. The drift–flux model, in which the relative velocity between the gas and liquid phases was estimated, generated better results than the homogeneous model. Drift–flux parameters in the tube bundle should be considered in future studies.

(ii) The added mass coefficient was obtained from quiescent two-phase flow as a function of void fraction. Using the added mass coefficient, the added stiffness coefficient converged to zero with decreasing nondimensional gap velocity. This overcame the contradiction in the added stiffness estimation without added mass, in which the added stiffness coefficient did not converge to zero with decreasing nondimensional gap velocity.

(iii) It was found that the equivalent added stiffness and damping coefficients did not depend on the tube amplitude significantly and nonlinearity was small in the excitation experiment of 15 Hz when the tube amplitude was 3 mm ($=0{\cdot}136D$) or less. This suggested the validity of the fluidelastic force coefficients obtained based on the data of amplitude of 3 mm.

(iv) Linearity did not exist when the tube displacement amplitude was 4·5 mm ($=0{\cdot}205D$) or more; remarkable nonlinearity appeared in the equivalent added damping coefficient. A method to estimate the limit-cycle amplitude of the fluidelastic vibration was proposed when only one tube in the tube bundle was able to vibrate in the lift direction. The amplitude could be obtained from the amplitude at which the equivalent added damping coefficient changed from negative to positive with increasing tube amplitude. Experimental verification is necessary in future studies.

REFERENCES

AXISA, F., VILLARD, B., GIBERT, R. J., HETSRONI, G. & SUNDHEIMER, P. 1984 Vibration of tube bundles subjected to air-water and steam–water cross-flow: preliminary results on fluid elastic instability. In *Symposium on Flow-Induced Vibrations*, Vol. 2: *Vibration of Arrays of Cylinders in Cross-Flow* (eds M. P. Païdoussis, M. K. Au-Yang & S. S. Chen), pp. 269–284. New York: ASME.

BAJ, F., PAYAN, T. & DE LANGRE, E. 2002 Scaling of damping induced by bubbly flow across tubes. *Journal of Fluids and Structures*, to appear.

CARLUCCI, L. N. 1980 Damping and hydrodynamic mass of a cylinder in simulated two-phase flow. *ASME Journal of Mechanical Design* **102,** 597–602.

CARLUCCI, L. N. & BROWN, J. D. 1983 Experimental studies of damping and hydrodynamic mass of a cylinder in confined two-phase flow. *ASME Journal of Vibration, Acoustics, Stress, and Reliability in Design* **105,** 83–89.

CHEN, S. S. 1991 Flow-induced vibrations in two-phase flow. *ASME Journal of Pressure Vessel Technology* **113,** 234–241.

CONNORS, H. J. 1970 Fluidelastic vibration of tube arrays excited by cross flow. In *Flow-Induced Vibration of Heat Exchangers* (ed D. D. Reiff), pp. 42–47. New York: ASME.

HARA, F. 1993 A review of damping of two-phase flows. *Proceeding of the ASME PVP Conference, Seismic Engineering,* PVP-Vol. 256-2, pp. 87–101. New York: ASME.

HARA, F. & KOHGO, O. 1986 Numerical approach to added mass and damping of a vibrating circular cylinder in a two-phase bubble fluid. *Proceedings of the International Conference on Computational Mechanics*, Vol. 2, pp. VII255–260.

INADA, F., KAWAMURA, K. & YASUO, A. 1996 Fluidelastic force measurements acting on a tube bundle in two-phase cross flow. In *Proceedings of the ASME PVP Conference, Flow-Induced Vibration* (ed M. J. Pettigrew), PVP-Vol. 328, pp. 81–87. New York: ASME.

INADA, F., KAWAMURA, K. & YASUO, A. 1997 Fluidelastic force measurements acting on a tube bundle in two-phase cross flow, fluidelastic forces acting on the oscillated tube and tubes surrounding the oscillated tube. In *Proceedings of the 4th International Symposium of Fluid–Structure Interactions, Aeroelasticity, Flow-Induced Vibration and Noise* (eds M. P. Paidoussis *et al.*), AD-Vol.53-2, pp. 357–364. New York: ASME.

ISHII, M. 1977 One-dimensional drift–flux model and constitutive equations for relative motion between phases in various two-phase flow regimes. *ANL-77–47*.

NAKAMURA, T., FUJITA, K. & KAWANISHI, K. 1992 Study on the vibrational characteristics of a tube array caused by two-phase flow—Part 2, Fluid elastic vibration. *ASME Journal of Pressure Vessel Technology* **114,** 479–485.

NAKAMURA, T., FUJITA, K., KAWANISHI, K. & SAITO, I. 1986*a* Study on flow induced vibration of a tube array by a two-phase flow—2nd report: large amplitude vibration by steam–water flow. *Transactions of the Japanese Society of Mechanical Engineers C* **52**–483, 2790–2795 (in Japanese).

NAKAMURA, T., YAMAGUCHI, N., TSUGE, A., FUJITA, K., SAKATA, K. & SAITO, I. 1986*b* Study on flow induced vibration of a tube array by a two-phase flow—1st report; large amplitude vibration by air-water flow. *Transactions of the Japanese Society of Mechanical Engineers C* **52-**473, 252–257 (in Japanese).

NAKAMURA, T., FUJITA, K., KAWANISHI, K., YAMAGUCHI, N. & TSUGE, A. 1995 Study on the vibrational characteristics of a tube array caused by two-phase flow. Part II. Fluid elastic vibration. *Journal of Fluids and Structures* **9,** 539–562.

PETTIGREW, M. J. & TAYLOR, C. E. 1994 Two-phase flow-induced vibration: An overview. *Journal of Pressure Vessel Technology* **116,** 233–253.

PETTIGREW, M. J., TAYLOR, C. E. & KIM, B. S. 1989a Vibration of tube bundles in two-phase cross-flow—Part 2: Fluidelastic instability. *ASME Journal of Pressure Vessel Technology* **111,** 478–487.

PETTIGREW, M. J., TROMP, J. H., TAYLOR, C. E. & KIM, B. S. 1989b Vibration of tube bundles in two-phase cross-flow—Part 1; hydrodynamic mass and damping. *Journal of Pressure Vessel Technology* **111,** 466–477.

TANAKA, H. & TAKAHARA, S. 1981 Flow-induced vibration of tube array in cross flow. *Journal of Sound and Vibration* **77,** 19–37.

ZUBER, N. & FINDLAY, J. A. 1965 Average volumetric concentration in two-phase flow systems. *Journal of Heat Transfer* **87,** 453–468.

APPENDIX NOMENCLATURE

C_0	distribution parameter of the drift–flux model
C_{axox}	added damping coefficient
$C_{a\mathrm{eq}}$	equivalent added damping coefficient
D	tube diameter
$F_{xox,0-p}$	amplitude from zero to peak of fluidelastic force for the forced oscillation frequency component
g	gravity acceleration
G	mass flux of the flow at the gap
j_G, j_L, j_T	volumetric flux densities of gas, liquid and mixture
K_{axox}	added stiffness coefficient
$K_{a\mathrm{eq}}$	equivalent added stiffness coefficient including added mass component
M_{axox}	added mass coefficient
P	pitch of the tube bundle
X_{0-p}	tube displacement amplitude from zero to peak
u_G, u_L	gas and liquid velocities
U_g, U_{gH}	mixture gap velocities in drift–flux model and homogeneous model
V_{Gj}	drift velocity of the drift–flux model
V_R, V_{RH}	nondimensional gap velocity in drift–flux model and homogeneous model

α	gas-phase void fraction
β	homogeneous void fraction
ρ_G, ρ_L	densities of gas and liquid phases
ρ, ρ_H	mixture densities in drift–flux model and homogeneous model
σ	surface tension constant
ϕ	phase difference between the tube vibration and fluidelastic force
Ω	frequency of tube oscillation